Journal of Nuclear Materials 382 (2008) 147–153

Contents lists available at ScienceDirect

Journal of Nuclear Materials

journal homepage: www.elsevier.com/locate/jnucmat

Effect of interatomic potential on the behavior of dislocation-defect interaction simulation in α-Fe

S.M. Hafez Haghighat *, J. Fikar, R. Schäublin

Ecole Polytechnique Fédérale de Lausanne (EPFL), Centre de Recherches en Physique des Plasmas, Association Euratom-Confédération Suisse, CH 5232 Villigen PSI, Switzerland

ARTICLE INFO

PACS:
61.80.Az
61.72.Lk
31.15.Qg

ABSTRACT

Molecular dynamics simulation is one of the most useful methods to model defect generation and subsequent change in mechanical properties in material that will suffer irradiation in the future fusion reactors. This work is aimed at showing the influence of the empirical interatomic potential for the Fe–Fe interaction on the simulated shearing of α-Fe containing one edge dislocation interacting with one nanometric void sitting on its glide plane. The recent potentials derived by Ackland et al. [G.J. Ackland, D.J. Bacon, A.F. Calder, T. Harry, Philosophical magazine a-physics of condensed matter structure defects and mechanical properties 75 (1997) 713], Mendelev et al. [M.I. Mendelev, S. Han, D.J. Srolovitz, G.J. Ackland, D.Y. Sun, M. Asta, Philos. Mag. 83 (2003) 3977] and Dudarev–Derlet [S.L. Dudarev, P.M. Derlet, J. Phys. Condens. Matter 17 (2005) 7097] are used to identify critical parameters. The stress–strain responses are obtained under imposed strain rate and at temperatures ranging from 10 to 700 K at constant volume. It appears that different potentials give different strengths and rates of decrease of obstacle strength with increasing temperature. Results are analyzed in terms of dislocation core structure and thermal expansion. Implications for the choice of the potential are given.

1. Introduction

Low activation ferritic-martensitic steels are being extensively studied since these alloys are considered to be candidate materials for the blanket and first wall of fusion reactors [1–9]. Although the ferrite-based steels are relatively resistant to swelling and maintain good fracture toughness at irradiation temperatures above about 700 K, they are prone to loss of ductility at lower irradiation temperatures [10]. This limits the mechanical performance and lifetime of these alloys under fusion irradiation conditions. However, the complexity of the microstructure of these alloys hinders a detailed analysis of the underlying microscopic mechanisms, and studies are presently focused on model alloys, starting with pure Fe and Fe–Cr alloys [11]. Hence, in this research, pure α-Fe and molecular dynamics (MD) simulation are utilized to investigate the irradiation-induced effects, in particular the void, on the mechanical properties of this material.

Multiscale modeling appears as a major tool for the description of plasticity of materials, which includes MD simulations. They are used extensively nowadays in the study of the interaction of a dislocation with an obstacle, for example, in the case of voids and Cu precipitates in Fe (bcc) [12–17] and stacking fault tetrahedron in Cu (fcc) [18–20]. Although different works dealt with strengthening of irradiation induced fcc and bcc materials by dislocation-obstacle interaction, there is still a lack of understanding about its temperature dependence, the effect of size and type of obstacle. Moreover, the impact of the chosen empirical potential on these phenomena is generally overlooked.

In this work we consider the strengthening of bcc Fe due to the interaction of a perfect edge dislocation and a nanometric void using different interatomic potentials, as a function of void size and temperature. Three different empirical interatomic Fe–Fe potentials, namely the ones by Ackland et al. [21], Mendelev et al. [22] and Dudarev and Derlet [23], were used, which in the following are called 'Ackland', 'Mendelev' and 'Dudarev–Derlet', respectively. The atomic structure of edge dislocation core for various interatomic potentials was evaluated. Simulations are conducted at constant volume under imposed strain rate and the stress–strain response is recorded. To investigate the effect of thermal expansion at elevated temperatures the simulation box size was adjusted to be stress free.

2. Simulation method

The simulation method, detailed in [24], is briefly described here. The first step in MD simulation is to create a sample with an edge dislocation and a cavity with specific size in a perfect bcc crystal. The dislocation was described using anisotropic elasticity of the continuum, which is implemented in code Disloc. The second step allows

* Corresponding author. Tel.: +41 56 310 2694; fax: +41 56 310 4529.
E-mail address: masood.hafez@psi.ch (S.M. Hafez Haghighat).

0022-3115/$ - see front matter © 2008 Elsevier B.V. All rights reserved.
doi:10.1016/j.jnucmat.2008.08.017

the dislocation to relax by conjugated gradient to form appropriate dislocation core structure. In the last step MD simulation allows the edge dislocation to glide toward the void under imposed strain rate, which is achieved by Moldy code. The dislocation glides under shear strain applied to upper part of sample crystal whereas the lower part is fixed. Fig. 1 illustrates the MD sample consisting of a box including one edge dislocation in [1 1 2] direction and a void centered on the dislocation slip plane, (1 1 0). The box is built up of several regions. In region denoted M atoms are mobile and follow Newton's equation. Periodic boundary conditions are applied along x and y. The upper region D is a layer of atoms, which control the deformation of the sample and it is constrained to remain static. Each atom in D is displaced in the y direction (arrow) by a fixed increment at each time step corresponding to the imposed strain rate. Region T is a thermal bath used to control the temperature of the sample by rescaling the velocity of atoms every 100 steps. It was shown that the temperature increase in the core of the gliding dislocation, is not important for the specimen when only one passage of the dislocation is considered [24]. Region S contains atoms that are static and anchor the sample and thus avoids its drift in the direction of the applied stress or strain.

In present work the simulation time step is set to 1 fs and total simulation time is around 500 ps. A 5 ps annealing prior to straining is performed to equilibrate temperature. The resulting dislocation speed is 60 m s^{-1}, following the selected imposed strain rate of $3 \cdot 10^{-8}$ fs^{-1}, and the simulation box contains about half a million Fe atoms. The simulations are performed at six temperatures (10, 100, 200, 300, 400, 500 and 700 K) and five different void diameters (1, 2, 3, 4 and 5 nm). Box size is fixed to 25 nm and 20 nm in y and z directions, respectively, but the size in x dimension varied with void size (13, 14, 15, 16 and 17 nm) to keep interspacing of the voids in the direction of the dislocation line constant due to periodic boundary condition.

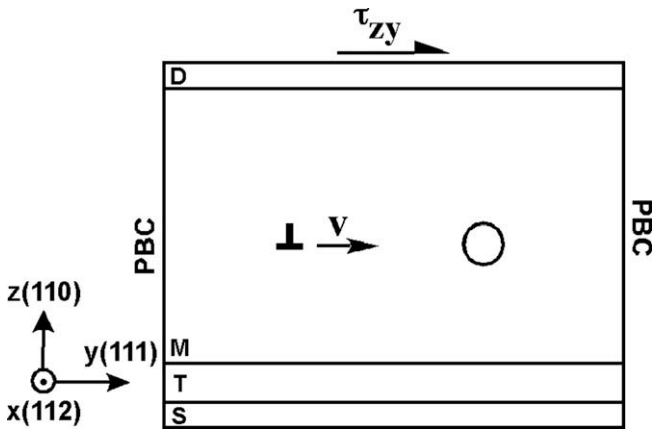

Fig. 1. Schematic view of simulation box containing an edge dislocation and a cavity. Imposed shearing, dislocation movement and different regions of the box are shown in this image. Periodic boundary condition are set in x and y directions.

The selected Fe–Fe potentials are the ones of Ackland et al. [21], Mendelev et al. [22] and Dudarev and Derlet [23], which are all using the embedded atom method [25], which implies a pair potential part and an 'embedding' part that depends on electronic density. Relative to Ackland potential, Mendelev provides better point defect properties, such as the correct relative formation energies between the <1 1 0> and the <1 1 1> self-interstitials, a critical topic in α-Fe and radiation damage. The Dudarev–Derlet potential provides the same improvement, relative to Ackland, and the inclusion of magnetic effects, such as the ferromagnetic transition upon lattice straining. Mendelev potential has the longest range, of 5th nearest neighbor, while the other two, Ackland and Dudarev, have range of 2nd and 3rd nearest neighbor. The nominal lattice parameter is 2.8665, 2.8553 and 2.8665 Å for the Ackland, Mendelev and Dudarev–Derlet potential, respectively. It should be noted that these empirical potentials are usually fitted at zero temperature, to an arbitrary selection of properties, which for those potentials include point defect properties and elastic constants. Simulation performed at finite temperatures should thus be taken with caution, in addition to the fact that MD simulations are approximate at temperatures below Debye temperature because of the inequality between the kinetic and potential energies. Our MD simulations are performed within these approximations.

3. Results and discussion

3.1. Temperature and size effect

Three stages of interaction of an edge dislocation with a 4 nm void at 200 K using Dudarev–Derlet Fe potential are illustrated in Fig. 2, which shows (Fig. 2(a)) the glide of dislocation towards the defect, prior to interaction, (Fig. 2(b)) attraction of the edge dislocation to defect in the vicinity of void and (Fig. 2(c)) release of dislocation after bowing out from void. Fig. 2(c) shows that the dislocation in bowing pulls two dislocation segments, pinned at the void, that have a near-screw character. Note that in these images only atoms having potential energy higher than chosen threshold energy are displayed. In Fig. 2(c) the shearing of the void by the edge dislocation is nearly complete. To have a clearer view of the shearing phenomenon cross cuts of the sheared void with different sizes are displayed (Fig. 3). These images show the way a cavity is sheared by passage of an edge dislocation, as it has been shown for void [13] and He bubble [24] using Ackland Fe interatomic potential. The shearing introduces a step in the void at the entry location where the dislocation first touches the void and at the exit location where the dislocation escapes from the void. Interestingly, the exit step occurs at a different height relative to the entry step. This event is evidenced by the horizontal line drawn in Fig. 3(d) showing the lower height of the exit step. This has been shown by Osetsky et al. [13] and explained as the result of the formation of a jog on the edge dislocation.

Fig. 4 shows the stress–strain curve of edge dislocation interaction with a 1 and 3 nm void at various temperatures obtained with

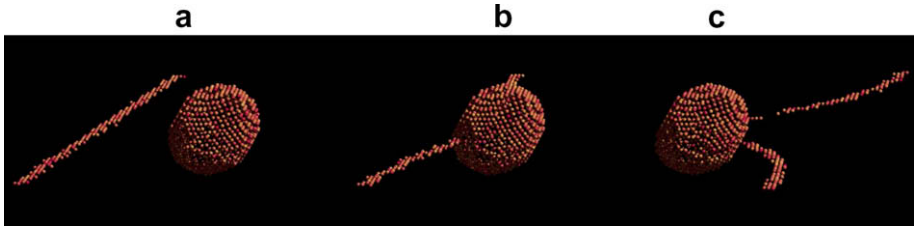

Fig. 2. Interaction of an edge dislocation and 4 nm void in bcc iron simulated by MD method at 200 K; (a) dislocation glide under imposed strain rate, (b) dislocation attraction in the vicinity of void and (c) dislocation bowing and shearing of the void.

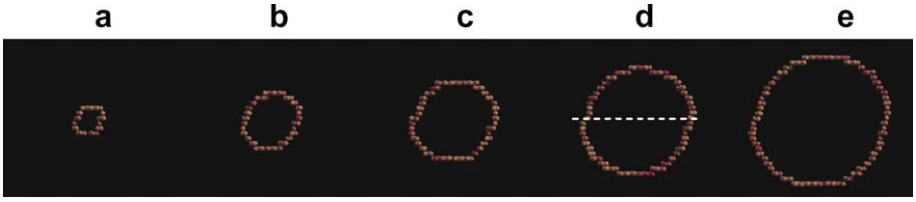

Fig. 3. Surface structure of voids after shearing of them by an edge dislocation passage for various sizes of (a) 1 nm, (b) 2 nm, (c) 3 nm, (d) 4 nm and (e) 5 nm. This images show step formation of one burgers vector in glide direction and difference in height of the step in entrance and exit of voids as it is appeared in image (d).

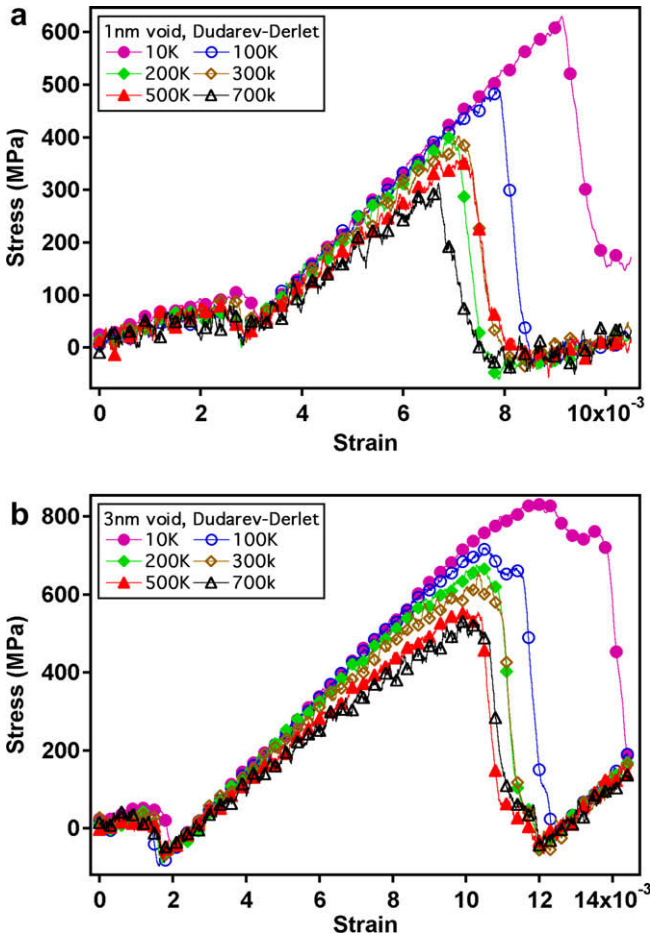

Fig. 4. The stress–strain curve of edge dislocation interaction with (a) 1 nm and (b) 3 nm void at various temperatures obtained by Dudarev–Derlet interatomic potential for Fe–Fe interaction.

Dudarev–Derlet potential. The release stress is decreasing with increasing of temperature. This behavior is comparable to the one obtained with the Ackland potential [26]. Fig. 5 shows release stresses as a function of void size and temperature. For all sizes, an increase of temperature results in softening. While the increase in void size has a strengthening influence on material, the strengthening rate tends to decrease with increasing void size.

Results are compared to the strengthening calculated in the frame of the elasticity of the continuum. The following relation, due to Bacon and Scattergood [27,28], based on the dislocation self interaction stress, is used,

$$\tau_c = \frac{Gb}{2\pi L}\left[\ln\frac{(D^{-1}+L^{-1})^{-1}}{b} + B\right], \qquad (1)$$

where G is the iron shear modulus for the <111>{110} system, which is 75.6 GPa according to our MD calculations using

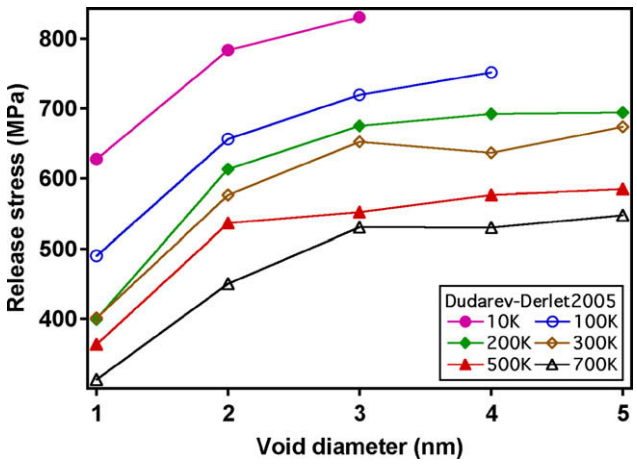

Fig. 5. Release stress vs. void diameter indicates that increasing of the void size at various temperatures has a strengthening effect on material.

Dudarev–Derlet potential, b is Burgers vector, L is the distance between void centers, D is the void diameter and B is a constant, which is 1.52 for a void [17]. Fig. 6 shows the values deduced from Eq. (1) together with the release stress obtained in the MD simulations of the present work. The plots show that at low temperatures, discrepancy of simulated results from theoretical evaluation are reasonable whereas at elevated temperatures this discrepancy becomes more pronounced, where the scaled critical stress decreases for different void sizes. At high temperatures, due to higher mobility of the near-screw segments, the dislocation release stress is lower

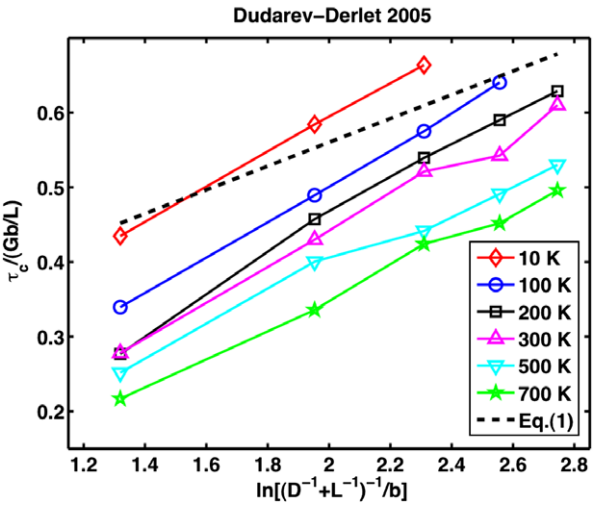

Fig. 6. Release stress, scaled by Gb/L vs. harmonic mean of obstacle spacing and void diameter at various temperatures using the Dudarev–Derlet potential. In this figure a dashed line plots the Eq. (1).

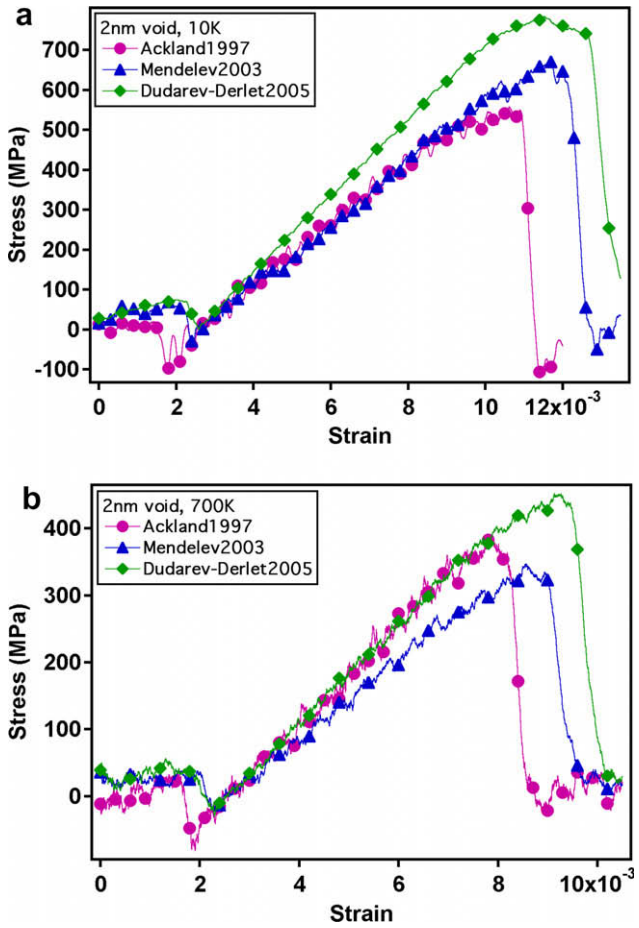

Fig. 7. The stress–strain curve of edge dislocation interaction with 2 nm void at (a) 10 K and (b) 700 K simulated using three different interatomic potentials for Fe–Fe interaction.

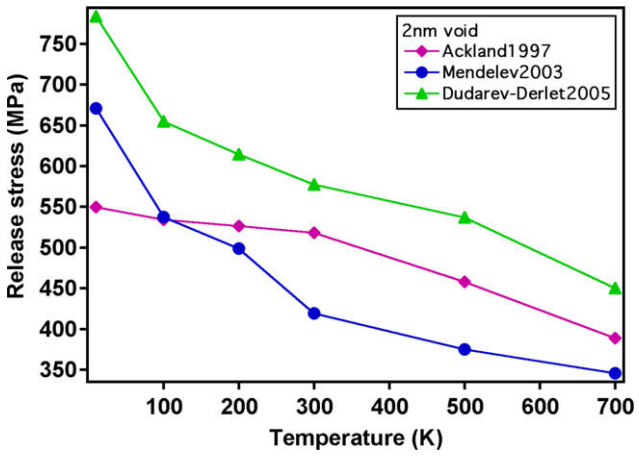

Fig. 8. Release stress of an edge dislocation from a 2 nm void vs. temperature using three different interatomic potentials for Fe–Fe interaction.

than at lower temperatures making it apart from the calculated critical stress using Eq. (1). One of the reasons that the results at various temperatures do not fit to the above equation might relate to the curvature and release angle of the dislocation from void, which depends on temperature and voids interspacing. While the elastic calculation does not take into account temperature dependence, it is interesting to consider the dislocation morphology temperature dependence, as observed in the MD simulations, and its possible impact on the release stress. Indeed, the small voids interspacing at elevated temperatures impedes the dislocation reaching a configuration where the pulled dislocation segments or arms are tangent to the void's surface, a necessary condition for the application of the Eq. (1). Note that it implies that the dislocation is released before the two arms reach a pure screw character (Fig. 2(c)).

3.2. Interatomic potential effect

This part of research is aimed at considering the impact of the Fe–Fe interatomic potential on strengthening effects of voids. Fig. 7 shows the stress–strain response with the edge dislocation and a 2 nm void at (Fig. 7(a)) 10 K and (Fig. 7(b)) 700 K as a function of the interatomic potential. Fig. 7(a) shows that Dudarev–Derlet potential leads to the highest release stress and strain. The release stress is almost 40% larger than the one obtained with Ackland. The second strongest interaction, in terms of release stress, is due to Mendelev potential, and Ackland potential leads to the weakest interaction. The increase of temperature (Fig. 7(b)) alters the ordering of potential dependent strengthening, as the Ackland potential leads to a stronger interaction than the one of Mendelev potential at high temperatures. Dudarev–Derlet still manifests the strongest interaction. In Fig. 8 the release stresses from the 2 nm void as a function of temperature and using different potentials are shown. It appears that at all temperatures from 10 K to 700 K Dudarev–Derlet potential shows the highest release stress, which is maximum at 10 K and is approximately 230 MPa higher than Ackland potential at this temperature. The other two potentials ranking switches their position at 100 K. Mendelev leads to a higher strengthening than Ackland below 100 K while at elevated tem-

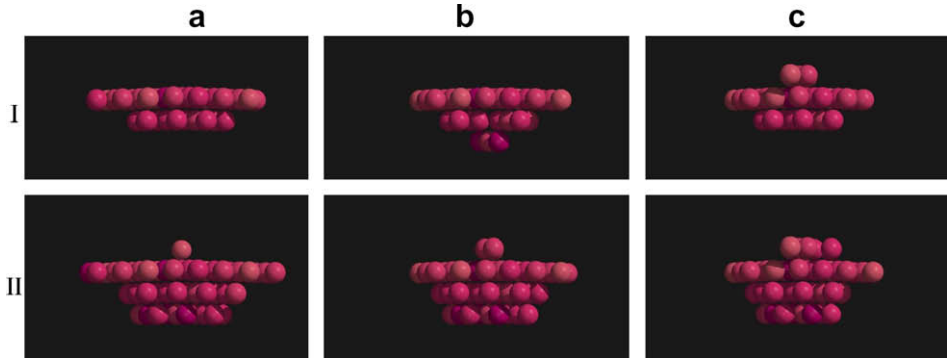

Fig. 9. High potential energy atoms in the core of an edge dislocation in α-Fe using (a) Ackland, (b) Mendelev, and (c) Dudarev–Derlet interatomic potentials. Two different threshold energies for display are used: (I) 50 meV and (II) 30 meV higher than the equilibrium potential energy (−4.308, −4.115 and −4.308 eV, respectively). Dislocation line is perpendicular to the paper.

peratures, beyond 200 K, Ackland leads to a stronger interaction than Mendelev.

The interaction of a dislocation with a defect relates to its core structure. Here we illustrate the core structure of edge dislocation constructed by three different Fe interatomic potentials. Fig. 9 shows in the edge dislocation line direction, <1 1 2>, the core structure of an edge dislocation obtained using various Fe interatomic potentials. The crystal with the dislocation has been relaxed by the method of conjugate gradients in Moldy, at 0 K, using the various potentials, namely (Figs. 9(a)) Ackland, (Figs. 9(b)) Mendelev and (Figs. 9(c)) Dudarev–Derlet. The dislocation core is in the centre of the images and atoms having higher potential energy than chosen threshold energy are illustrated. The threshold energy has a value of 50 meV, Figs. 9(I), and 30 meV, Figs. 9(II), higher than the equilibrium potential energy of an atom for each of interatomic potentials. The displayed atoms are the ones from the 6 atomic planes found along <1 1 2> in a single unit cell of Fe, as depicted in Fig 10. Fig. 10 shows a schematic sketch of {1 1 0} plane of bcc-Fe lattice having <1 1 2> direction and {1 1 2} planes depicted. Inspection of these illustrations reveals that the core structure obtained from Ackland potential gives the most compact core normal to the glide plane relative to others and it is spread only in the glide direction, whereas Mendelev and Dudarev–Derlet spread the core normal to the glide plane. It could explain why Ackland potential gives the lowest release stresses in edge dislocation-void interaction at low temperatures. Dudarev–Derlet gives the most spread core, which expands above the glide plane together with some bilateral asymmetry relative to the dislocation extra plane, Fig. 9(IIc). It could explain the fact that Dudarev–Derlet potential induces the highest release stress. However, more detailed investigations, in particular on the screw dislocation segments core structure, are required.

3.3. Effect of thermal expansion

Our MD simulations are usually performed using constant volume and the lattice parameter of α-Fe corresponding to the selected potential. Here we consider the effect of thermal expansion on the stress–strain response. The lattice parameter that corresponds to the required simulation temperature was deduced using an iterative method. A perfect $10 \times 10 \times 10$ unit cells simulation box is selected. An anneal is performed by MD under periodic boundary conditions by imposing a temperature gradient and a volume that is varied by altering the lattice parameter. The temperature corresponding to the selected lattice parameter is attained when the pressure in the box reaches zero. Fig. 11 shows the thermal expansion deduced from this method using the (Fig. 11(a)) Ackland, (Fig. 11(b)) Mendelev and (Fig. 11(c)) Dudarev–Derlet potentials. These graphs indicate a normal behavior of the thermal expansion of α-Fe for Ackland and Mendelev potentials, with a monotonous increase with increasing temperature, but an

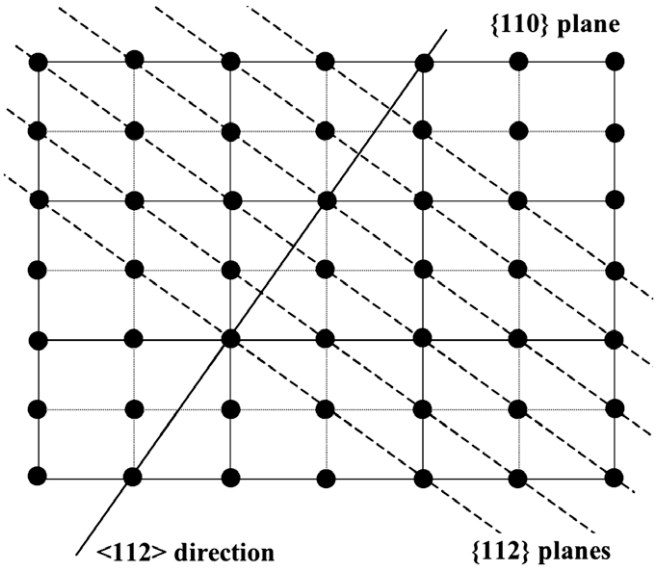

Fig. 10. Schematic lattice structure of {1 1 0} plane of bcc Fe showing dislocation direction in <1 1 2> directions and six atomic planes in each lattice repetition in dislocation direction.

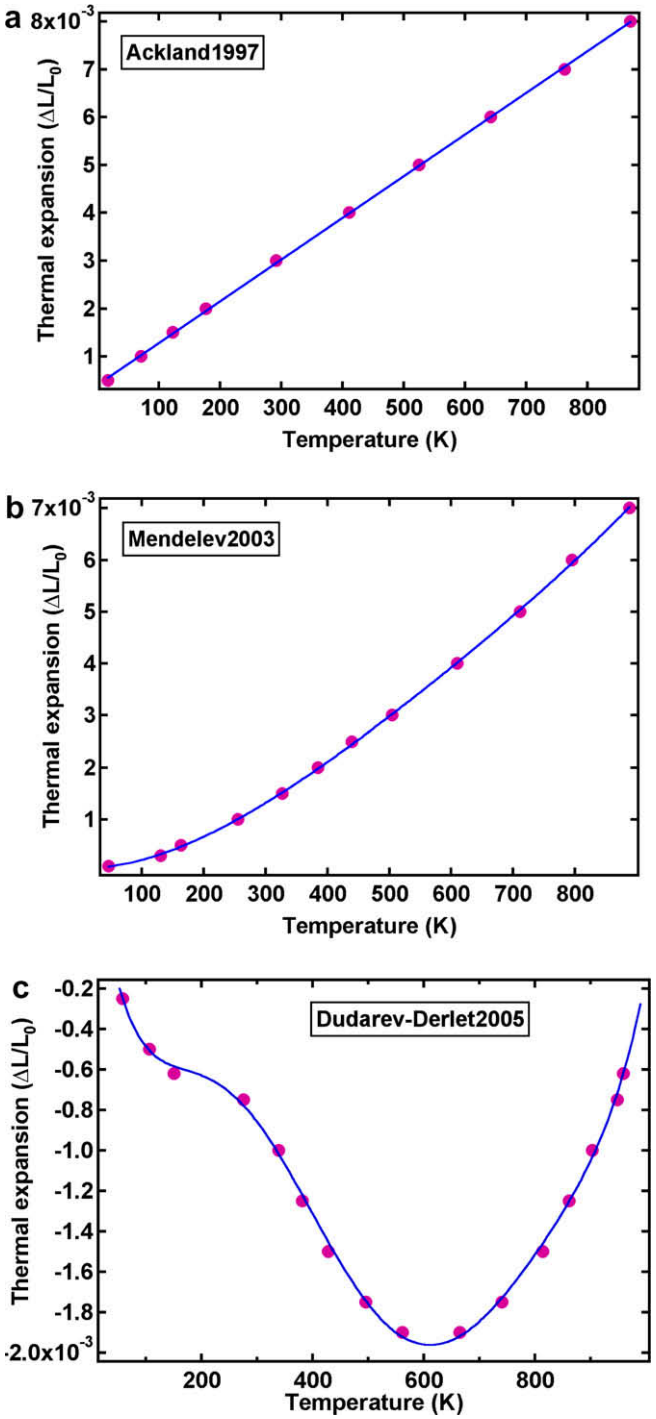

Fig. 11. Thermal expansion of bcc Fe at various temperatures below 1000 K achieved by three different Fe–Fe interatomic potentials; (a) Ackland, (b) Mendelev and (c) Dudarev–Derlet.

abnormal contraction of α-Fe for Dudarev–Derlet with a minimum around 600 K. Values of the obtained thermal expansion coefficients, α, deduced from $\Delta L/L_0 = \alpha T$, and the experimental values [29] are presented in Table 1. Ackland potential results are closer to experimental values than the other two potentials in the temperature range from 300 to 400 K.

Fig. 12 shows the release stress and strain for the interaction of an edge dislocation with a 2 nm void obtained with the nominal lattice parameter or 'original a_0' and the one, so-called 'adjusted a_0', adjusted to the thermal expansion coefficient corresponding to the potentials, Ackland (Fig. 12(a)) and Dudarev–Derlet (Fig. 12(b)). Fig. 12(a) shows that up to 300 K there is almost no effect of the adjustment of lattice parameter on the strengthening of material, while at higher temperatures, such as 700 K, the adjustment in lattice parameter leads to a higher release stress and strain than the ones derived with the nominal lattice parameter. The observed underestimate in the results of 700 K is actually a consequence of the thermal strain in the simulation lattice created by the nominal lattice parameter, which is too short at high temperature. At 700 K the lattice is compressed and thus eases the dislocation glide, because of the reduction of depth of the Peierls' valleys, and the release stress and strain of dislocation from the defect are decreased. For Dudarev–Derlet potential we observed almost no underestimation in release stress and strain, which might be due to its negative thermal expansion or due to smaller absolute value of the thermal expansion, when compare to Ackland potential (see Figs. 11(a) and (c)). On the basis of these investigation one may conclude that using the nominal or a constant lattice parameter in numerical simulations may be reasonable up to moderate temperatures but going to higher temperatures requires setting the lattice parameter to the adequate value.

Table 1
Thermal expansion coefficient obtained from three different Fe–Fe interatomic potentials and experimental results in the range of 300–400 K

Reference	α ($\times 10^{-6}$ K^{-1})
Ackland [21]	8.7
Mendelev [22]	8
Dudarev–Derlet [23]	−4.6
Experiments	12–13 [29]

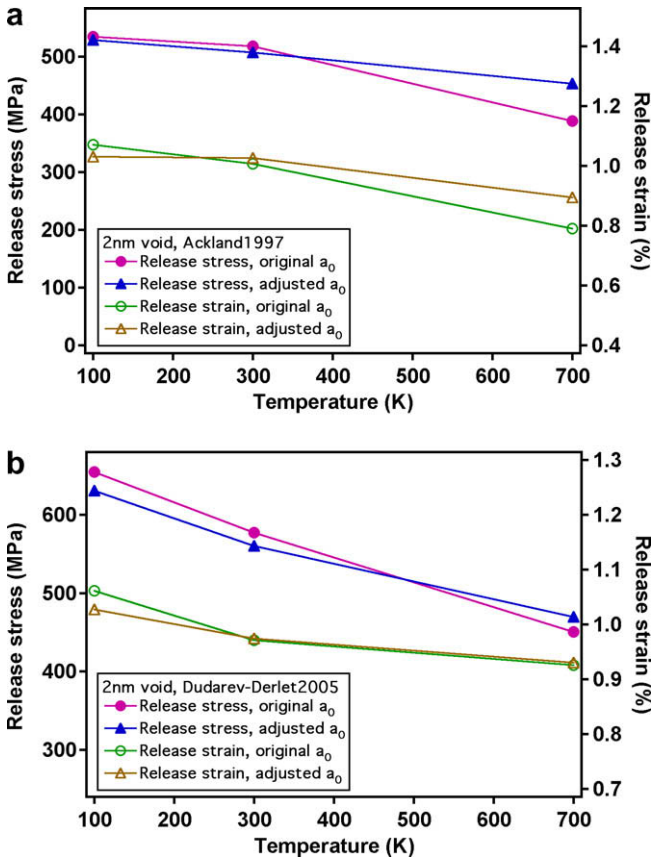

Fig. 12. Release stress of an edge dislocation from a 2 nm void at three different temperatures and using constant and adjusted box size, to eliminate the thermal stresses, for two different Fe–Fe interatomic potentials; (a) Ackland and (b) Dudarev–Derlet.

4. Conclusion

In this work we tried by MD simulations to show the influence of the defect size, temperature and empirical interatomic potential on the simulation of the shearing of α-Fe crystal containing an edge dislocation and a void. The recent potentials derived by Ackland et al. [21], Mendelev et al. [22] and Dudarev–Derlet [23] are used to identify critical parameters. The main conclusions of this study, performed within the approximations of MD simulations, are the following:

1. Using all potential it was revealed that with increasing temperature the interaction of an edge dislocation with a nanometric void softens. Results obtained by Dudarev–Derlet potential showed the temperature effect does not depend on the void size.
2. The increase in void size strengthens the material but the strengthening rate tends to decrease with increasing size, which is in agreement with the hardening deduced from elasticity theory.
3. The use of three different and recent interatomic potentials for Fe–Fe interaction results in significant differences in the edge dislocation-void interaction. The release stress difference tops at 230 MPa at 10 K using Dudarev–Derlet relative to Ackland, which gives a release stress of 783 MPa. The simulations revealed that Dudarev–Derlet potential predict the strongest dislocation-void interaction relative to the other two potentials whereas Mendelev and Ackland potentials give mixed behavior depending on temperature.
4. The thermal expansion of α-Fe using three different potentials was scrutinized. Results with Ackland and Mendelev potentials showed a normal thermal expansion behavior with a lower thermal expansion coefficient than experimental values but Dudarev–Derlet predicts a contractive thermal expansion with a minimum around 600 K.
5. When using the lattice parameter appropriate to the requested temperature it appears that at elevated temperatures the results of simulations might deviate from the ones performed with the nominal lattice parameter because of the subsequent thermal stresses in the simulation box, which could ease the dislocation passage through the defect due to the compaction of the lattice.

Acknowledgments

This work, supported by the European Communities under the contract of Association between EURATOM/Swiss Confederation was carried out within the framework of the European Fusion Development Agreement. The views and opinions expressed herein do not necessarily reflect those of the European Commission. PSI is acknowledged for the overall use of facilities.

References

[1] V.K. Shamardin, V.N. Golovanov, T.M. Bulanova, A.V. Povstianko, A.E. Fedoseev, Y.D. Goncharenko, Z.E. Ostrovsky, J. Nucl. Mater. 272 (1999) 155.
[2] K. Shiba, M. Suzuki, A. Hishinuma, J. Nucl. Mater. 237 (1996) 309.
[3] Y. Kohno, A. Kohyama, T. Hirose, M.L. Hamilton, M. Narui, J. Nucl. Mater. 272 (1999) 145.
[4] R. Lindau, A. Moslang, M. Rieth, M. Klimiankou, E. Materna-Morris, A. Alamo, A.A.F. Tavassoli, C. Cayron, A.M. Lancha, P. Fernandez, N. Baluc, R. Schaublin, E. Diegele, G. Filacchioni, J.W. Rensman, B. van der Schaaf, E. Lucon, W. Dietz, Fusion Eng. Design 75-9 (2005) 989.
[5] R. Schaeublin, T. Leguey, P. Spatig, N. Baluc, M. Victoria, J. Nucl. Mater. 307 (2002) 778.
[6] E. Lucon, R. Chaouadi, M. Decreton, J. Nucl. Mater. 329-33 (2004) 1078.
[7] Y. Dai, S.A. Maloy, G.S. Bauer, W.F. Sommer, J. Nucl. Mater. 283 (2000) 513.
[8] R. Schaublin, M. Victoria, J. Nucl. Mater. 283 (2000) 339.
[9] P. Spatig, R. Schaublin, S. Gyger, M. Victoria, J. Nucl. Mater. 263 (1998) 1345.
[10] B.N. Singh, A. Horsewell, P. Toft, J. Nucl. Mater. 272 (1999) 97.
[11] M.I. Luppo, C. Bailat, R. Schaublin, M. Victoria, J. Nucl. Mater. 283 (2000) 483.
[12] Y.N. Osetsky, D.J. Bacon, Modell. Simul. Mater. Sci. Eng. 11 (2003) 427.
[13] Y.N. Osetsky, D.J. Bacon, V. Mohles, Philos. Mag. 83 (2003) 3623.
[14] Y.N. Osetsky, D.J. Bacon, Mater. Sci. Eng. Struct. Mater. Prop. Microstruct. Process. 400 (2005) 374.
[15] Y.N. Osetsky, D.J. Bacon, J. Nucl. Mater. 323 (2003) 268.
[16] D.J. Bacon, Y.N. Osetsky, Mater. Sci. Eng. Struct. Mater. Prop. Microstruct. Process. 365 (2004) 46.
[17] D.J. Bacon, Y.N. Osetsky, Mater. Sci. Eng. Struct. Mater. Prop. Microstruct. Process. 400 (2005) 353.
[18] B.D. Wirth, M.J. Caturla, T.D. de la Rubia, T. Khraishi, H. Zbib, Nucl. Instrum. and Meth. Phys. Res. B Beam Interactions Mater. Atoms 180 (2001) 23.
[19] B.D. Wirth, G.R. Odette, J. Marian, L. Ventelon, J.A. Young-Vandersall, L.A. Zepeda-Ruiz, J. Nucl. Mater. 329-33 (2004) 103.
[20] J. Marian, B.D. Wirth, R. Schaublin, G.R. Odette, J.M. Perlado, J. Nucl. Mater. 323 (2003) 181.
[21] G.J. Ackland, D.J. Bacon, A.F. Calder, T. Harry, Philos. Mag. Phys. Condens. Matter Struct. Defect Mech. Prop. 75 (1997) 713.
[22] M.I. Mendelev, S. Han, D.J. Srolovitz, G.J. Ackland, D.Y. Sun, M. Asta, Philos. Mag. 83 (2003) 3977.
[23] S.L. Dudarev, P.M. Derlet, J. Phys. Condens. Matter 17 (2005) 7097.
[24] R. Schäublin, Y.L. Chiu, J. Nucl. Mater. (2007), doi:10.1016/j.jnucmat.2007.01.187.
[25] M.S. DAW, M.I. Baskes, Phys. Rev. B 29 (1984) 6443.
[26] S.M. Hafez Haghighat, R. Schaeublin, Molecular dynamics modeling of cavity strengthening in irradiated iron, in: Proceeding: Multiscale Materials Modeling, Freiburg-Germany, September 2006, p. 729.
[27] R.O. Scattergood, D.J. Bacon, Acta Metall. 30 (1982) 1665.
[28] D.J. Bacon, U.F. Kocks, Scatterg. Ro, Philos. Mag. 28 (1973) 1241.
[29] ASM Materials Data Series, Thermal expansion, in: Fran Cverna (Eds.), Thermal Properties of Metals, Springer, USA, 2002, p. 9.